

(HUANJING KEXUE)

# ENVIRONMENTAL SCIENCE

第39卷 第3期

Vol.39 No.3

2018

\_\_\_\_ 中国科学院生态环境研究中心 主办

斜学出版社出版



## 环龙科豆 (HUANJING KEXUE)

#### ENVIRONMENTAL SCIENCE

第39 卷 第3期 2018年3月15日

#### 次

## 二氧化钛对地下水中砷硅的吸附及再生回用

马文静1, 阎莉2,3, 张建锋1\*

(1. 西安建筑科技大学环境与市政工程学院,西安 710055; 2. 中国科学院生态环境研究中心,北京 100085; 3. 中国科学院大学,北京 100049)

摘要:二氧化钛( $\mathrm{TiO_2}$ )材料作为性能优异的吸附材料被广泛应用于地下水砷( $\mathrm{As}$ )的去除中.结果表明,地下水中共存硅离子( $\mathrm{Si}$ )会占据  $\mathrm{TiO_2}$  的吸附位点,从而影响  $\mathrm{As}$  的吸附及  $\mathrm{TiO_2}$  材料的再生回用.本文通过同步辐射扩展 X 射线吸收精细结构 ( $\mathrm{EXAFS}$ )研究了  $\mathrm{Si}$  对  $\mathrm{As}$  微观吸附机制的影响,表明  $\mathrm{Si}$  的存在不会影响  $\mathrm{As}$  在  $\mathrm{TiO_2}$  上的吸附构型.衰减全反射傅里叶变换红外光谱( $\mathrm{ATR}$ - $\mathrm{FTIR}$ )原位研究表明  $\mathrm{Si}$  在  $\mathrm{TiO_2}$  表面形成  $\mathrm{Si}$  单体、低聚体和多聚体,从而竞争  $\mathrm{As}$  的吸附位点,同时增加  $\mathrm{TiO_2}$  再生的难度.为了实现  $\mathrm{TiO_2}$  材料的高效再生,本研究进一步考察了氟化钠( $\mathrm{NaF}$ )对  $\mathrm{TiO_2}$  表面  $\mathrm{Si}$  的脱附效果,发现  $\mathrm{NaF}$  可以有效地洗脱  $\mathrm{Si}$ ,再生后的  $\mathrm{TiO_2}$  吸附性能稳定.  $\mathrm{ATR}$ - $\mathrm{FTIR}$  光谱原位分析发现, $\mathrm{NaF}$  的加入可有效脱附  $\mathrm{TiO_2}$  表面的  $\mathrm{Si}$  单体和多聚体.当利用  $\mathrm{NaF}$  和  $\mathrm{NaOH}$  共同洗脱  $\mathrm{TiO_2}$  表面的  $\mathrm{As}$  和  $\mathrm{Si}$  时,3 次循环中  $\mathrm{As}$  的脱附率为  $\mathrm{86.8\%}$  ~ 100.3%, $\mathrm{Si}$  的脱附率为  $\mathrm{67.9\%}$  ~ 82.0%,本研究为地下水砷硅共吸附材料的再生提供了一种有效方法。

关键词:二氧化钛; 砷硅共存; 硅聚合体; 再生回用; 微观机制

中图分类号: X523 文献标识码: A 文章编号: 0250-3301(2018)03-1241-07 DOI: 10.13227/j. hjkx. 201706112

# Groundwater Arsenic and Silicate Adsorption on ${\rm TiO_2}$ and the Regeneration of ${\rm TiO_2}$

MA Wen-jing<sup>1</sup>, YAN Li<sup>2,3</sup>, ZHANG Jian-feng<sup>1,4</sup>

(1. School of Environmental and Municipal Engineering, Xi'an University of Architecture & Technology, Xi'an 710055, China; 2. Research Center for Eco-Environmental Science, Chinese Academy of Sciences, Beijing 100085, China; 3. University of Chinese Academy of Sciences, Beijing 100049, China)

Abstract: Titanium dioxide (TiO<sub>2</sub>) was widely used to remove arsenic (As) from groundwater due to its excellent properties. Previous studies show that the coexisting silicate ions (Si) could occupy the available surface sites of TiO<sub>2</sub> and further inhibit As adsorption and TiO<sub>2</sub> regeneration. To investigate the effect of Si adsorption on the As molecular surface structure, an extended X-ray absorption fine structure (EXAFS) analysis was conducted in this work. The results indicated that the presence of Si exhibited no impact on the As adsorption configuration on TiO<sub>2</sub>. In situ attenuated total reflectance Fourier transform infrared (ATR-FTIR) spectroscopy results demonstrated that the polymerization of Si that formed on the TiO<sub>2</sub> surface compete with As adsorption sites, increasing the difficulty for TiO<sub>2</sub> regeneration. To effectively regenerate TiO<sub>2</sub>, the removal efficiency of Si polymers on TiO<sub>2</sub> via sodium fluoride (NaF) was studied. The results showed that NaF could remove Si monomer and polymer from TiO<sub>2</sub>, and the regenerated TiO<sub>2</sub> could be reused with a stable adsorption performance. In situ ATR-FTIR spectroscopy suggested that NaF desorbed the Si monomer and polymer effectively. When spent TiO<sub>2</sub> was regenerated with NaOH and NaF in three treatment cycles, As and Si desorption rates were 86. 8% -100. 3% and 67. 9% -82. 0%, respectively. The present study provides a new insight into regenerating absorbents with coadsorbed As and Si in groundwater.

Key words: titanium dioxide; coexisting arsenic and silicate; silicate polymer; regeneration and reuse; molecular-level study

砷(As)是一种毒性极强的类金属元素,具有广泛的生物效应,早在1978年已被国际癌症研究中心(IRAC)列为第一类致癌物<sup>[1,2]</sup>.长期饮用高砷水(>10 μg·L<sup>-1</sup>)会对人体健康造成严重危害<sup>[3~5]</sup>.因此,高效经济地处理高砷地下水显得至关重要.吸附过滤是当前处理地下水砷污染的主流技术<sup>[6,7]</sup>.二氧化钛材料因其高效的吸附活性和化学稳定性已成功用于高砷地下水的去除中<sup>[8~11]</sup>.地下水基质复杂,共存离子的存在会影响砷的吸附<sup>[12,13]</sup>.其中,硅离子以硅酸(H<sub>4</sub>SiO<sub>4</sub>)的形式广

泛存在于地下水中<sup>[14]</sup>.由于其与 TiO<sub>2</sub> 表面具有较强的亲和力,可以在 TiO<sub>2</sub> 表面发生聚合作用形成稳定的 Si 单体和多聚体而阻碍砷的吸附<sup>[15~17]</sup>.此外, Si 在 TiO<sub>2</sub> 上长期形成的稳定聚合体很难被HCl 或 NaOH 完全洗脱,这也是再生后 TiO<sub>2</sub> 对 As 吸附效率变低的主要原因之一<sup>[18]</sup>.因此亟需开发

收稿日期: 2017-06-13; 修订日期: 2017-08-11

基金项目: 国家自然科学基金项目(41373123); 陕西省自然科学基础研究计划项目(2016JM5080)

作者简介: 马文静(1992~), 女, 硕士研究生, 主要研究方向为高 神地下水处理, E-mail: mawj2017@163.com

\* 通信作者,E-mail:zhangjianfeng@ xauat.edu.cn

高效可行的 Si 脱附方法以提高吸附材料的再生利用率.

本文采用同步辐射的扩展 X 射线吸收精细结构(EXAFS)手段研究了 Si 对 As 微观吸附机制的影响,并利用衰减全反射傅里叶变换红外光谱(ATR-FTIR)手段探究了 Si 在 TiO<sub>2</sub> 表面的原位吸附行为,提出了采用一种新型 NaF 脱附 Si 的方法,探究其对 Si 的脱附效果,并利用 ATR-FTIR 光谱研究 NaF对 TiO<sub>2</sub> 表面 Si 的微观脱附效果. 最后探究了 TiO<sub>2</sub>表面 As 和 Si 的脱附效果及 TiO<sub>2</sub>的再生情况,以期为实际高砷地下水处理中 TiO<sub>2</sub>的高效回收利用提供指导.

#### 1 材料与方法

#### 1.1 实验仪器

电感耦合等离子体发射光谱仪(ICP-OES, Optima 2000 DV, Perkin Elmer Co, USA);原子吸收光谱仪(FAAS, Perkin-Elmer AAS-800);电子天平(ME104);pH计(FE20);同步辐射拓展 X 射线吸收谱(Extended x-ray absorption fine structure, EXAFS);傅里叶变换红外光谱仪(FTIR: Thermo-Nicolet Nexus 6700)和衰减全反射(ATR: PIKE Tech)附件.

#### 1.2 实验试剂及材料

实验所用九水硅酸钠、砷酸钠、氢氧化钠、氟化钠、浓盐酸均为分析纯,购自国药集团化学试剂有限公司. 为模拟实际高砷地下水中基质环境,使用陈化自来水配制  $100~\text{mg}\cdot\text{L}^{-1}$ 的硅储备溶液. 由于 As(V)是含氧水体中砷的主要形态,同样使用自来水配制  $100~\text{mg}\cdot\text{L}^{-1}$  Si 和  $1~\text{mg}\cdot\text{L}^{-1}$  As(V)的共存储备溶液.

#### 1.3 实验方法

#### 1.3.1 As 边 EXAFS 谱图研究

单神吸附样品:采用 30 mg·L<sup>-1</sup> As(V)储备溶液与 5 g·L<sup>-1</sup>颗粒 TiO<sub>2</sub> 在 pH = 7 条件下充分混合 24 h,砷硅共吸附样品:采用 30 mg·L<sup>-1</sup>As(V)和 112 mg·L<sup>-1</sup> Si 的砷硅共存溶液与 5 g·L<sup>-1</sup>颗粒 TiO<sub>2</sub> 在 pH = 7 条件下充分混合 24 h. 反应后离心分离得到固体样品,经冷冻干燥后研磨过筛(200 目). 将粉末样品置于 Kapton 胶带密封,用于 EXAFS 的检测. 砷(11 867 eV)的 K 边 EXAFS 谱图的采集在台湾新竹同步辐射光源线站 01C1 线站进行. 砷的 K 边 EXAFS 谱采用 Lytle 检测器从边前 – 200 eV 采集到边后1 000 eV. 每个样品采集 3~9 次,最终谱图

处理及拟合采用所有谱图的平均. EXAFS 谱图处理 及拟合过程采用 Demeter 软件包中的 Athena 及 Artemis 程序进行.

#### 1.3.2 TiO<sub>2</sub> 颗粒的制备

颗粒 TiO<sub>2</sub> 采用水解硫酸氧钛的方法制备<sup>[19]</sup>. 具体方法为:将 300 g 硫酸氧钛(TiOSO<sub>4</sub>)溶于 2 L 去离子水中,在 4℃冰水浴中机械搅拌条件下,用 200 g·L<sup>-1</sup>的氢氧化钠(NaOH)溶液调节 pH 至 7.5. 用去离子水反复清洗悬浊液,直到悬浊液的电导率小于 100 μS·cm<sup>-1</sup>,即得到偏钛酸浆液. 取偏钛酸浆液 800 g,加入 80 mL 1 g·L<sup>-1</sup>的聚乙烯醇(PVA)溶液,90℃水浴封口加热搅拌 3h 后再暴露于空气中,以利于浆液中水分的蒸发. 当偏钛酸浆液趋于块状时用研钵将其磨碎成小颗粒,过 40~60 目筛后于 60℃干燥 6 h,得到 TiO<sub>2</sub> 颗粒,其粒径为 0. 25~0. 38 mm.

#### 1.3.3 脱附 Si 动力学实验

TiO<sub>2</sub>吸附 Si 实验:室温条件下,分别称取 0.2~g TiO<sub>2</sub>加入  $15~\uparrow$  50 mL 离心管中,然后加入 40~mL Si 溶液  $(100~\text{mg}\cdot\text{L}^{-1})$ ,用 HCl 和 NaOH 调节溶液 pH = 7. 吸附 60~h 后,固液分离,将溶液过  $0.45~\mu\text{m}$  滤膜,利用电感耦合等离子体发射光谱仪 (ICPOES)测定溶液中的 Si 浓度.固体 TiO<sub>2</sub> 颗粒进行下一步脱附实验.

NaF 脱附 Si 动力学实验:将 15 个装有上述固体 TiO<sub>2</sub> 颗粒的离心管分为 5 组. 5 组分别加入 50 mL pH = 5 的 10、50、100、200、500 mg·L<sup>-1</sup>的 NaF 溶液,隔时取样,12 h 后停止脱附. 固液分离,将溶液过 0.45  $\mu$ m 滤膜,利用 ICP-OES 测定溶液中的 Si 浓度. 固体 TiO<sub>2</sub> 颗粒重新吸附 Si 平衡后,重复上述脱附动力学实验,最终得到三次 NaF 脱附 Si 的实验数据.

#### 1.3.4 原位红外光谱分析

研磨  $TiO_2$  颗粒过 400 目筛,配制  $3.5 \text{ g·L}^{-1}$ 的  $TiO_2$  悬浊液. 取 0.7 mL 的  $3.5 \text{ g·L}^{-1}$ 的  $TiO_2$  悬浊液滴加在  $56 \text{ mm} \times 10 \text{ mm}$  ZnSe 晶体上,在空气中晾干后使用. 采用 MCT 检测器与  $45^{\circ}$ 角 ZnSe 晶体进行实验,采集次数为 256 次,分辨率为  $4 \text{ cm}^{-1}$ . 实验过程中,先用 pH = 5 的  $0.585 \text{ g·L}^{-1}$  NaCl 溶液以  $0.25 \text{ mL·min}^{-1}$ 的流速在  $TiO_2$  薄膜上平衡 3 h 后;将溶液换为  $20 \text{ mg·L}^{-1}$  Si,随时间变化采集谱图;Si 溶液反应 3.5 h 后将溶液换为  $50 \text{ mg·L}^{-1}$  NaF 溶液,随时间变化采集红外谱图,3 h 后结束采集. 利用 0 mmic 软件的基线校正功能进行基线校正后,采

用 Peakfit v. 4. 12 软件分峰, 并利用 Omnic 软件的二维红外光谱功能绘制 Si 在 TiO<sub>2</sub> 上原位吸附的二维谱图.

#### 1.3.5 NaF 与 NaOH 共同再生 TiO,

砷硅共吸附实验:室温条件下,分别称取 0.2~g  $TiO_2$ 加入 3~f 50~mL 离心管中,然后加入 40~mL 的  $100~mg \cdot L^{-1}$  Si 和  $1~mg \cdot L^{-1}$  As( V) 的共存储备溶液,用 HCl 和 NaOH 调节溶液 pH = 7. 平衡 60~h 后,固液分离,将溶液过  $0.45~\mu m$  滤膜,利用 ICPOES 测定溶液中的 Si 浓度,利用原子吸收光谱仪测定溶液中的 As 浓度. 固体  $TiO_2$  颗粒进行下一步再生实验.

TiO<sub>2</sub> 的再生回用:在 3 个装有上述固体 TiO<sub>2</sub> 颗粒的离心管中加入 20 mL 的 80 g·L<sup>-1</sup> NaOH 溶液. 反洗 4 h 后,固液分离,将溶液过 0.45  $\mu$ m 滤膜,测定溶液中的 As 和 Si 浓度. 将固体 TiO<sub>2</sub> 颗粒用超纯水和 18 g·L<sup>-1</sup> HCl 溶液简单冲洗后,加入 30 mL 的 200 mg·L<sup>-1</sup> NaF 溶液. 反洗 6 h 后,固液分离,测定溶液中的 As 和 Si 浓度. 固体 TiO<sub>2</sub> 颗粒重新吸附 As 和 Si 平衡后,重复上述的再生回用实验,最终得到 TiO<sub>2</sub> 的 3 次再生实验数据.

#### 2 结果与讨论

#### 2.1 Si 对 As 微观吸附机制的影响

TiO, 对单砷、砷硅共存溶液 As 的吸附量分别 为 5.12 mg·g<sup>-1</sup>、2.78 mg·g<sup>-1</sup>, Si 的吸附量为 15. 34 mg·g<sup>-1</sup>, 较大的 Si 吸附量影响了 As 的吸附. 为研究 Si 对 As 微观吸附机制的影响, 分别研究了 单砷和砷硅吸附在颗粒 TiO, 上的砷 K 边 EXAFS 谱 图,拟合结果如图1和表1所示.图1中位于1.68 ~1.69 nm 处的最强峰为 As—O 振动, 配位数为 4, 与As(V)的正四面体结构吻合. 在As(V)吸附样品 中, 第二层峰为 As—Ti 振动, 键长为 33 nm, 配位数 为 0. 8 个 Ti 原子. As—Ti 距离说明 As( V) 以双齿双 核形式吸附在 TiO, 上,与文献[20]的报道一致. 在 As(V)与 Si 共吸附样品中, 第二层拟合得到的 As— Ti 键长为 3.32 Å, 配位数为 0.4 个 Ti 原子, 这与单 砷吸附样品的拟合结果相似,说明As(V)与Si共存 时(Si/As 摩尔比为10), Si 的存在不会影响 As(V) 在 TiO2上的微观吸附构型. Si 对As(V)吸附的阻碍 作用可能是由于竞争吸附位点引起的, 这与文献 [20, 21]的报道结果吻合.

表 1 单砷和砷硅吸附在颗粒 TiO<sub>2</sub> 上的砷 K 边 EXAFS 谱图拟合参数

Table 1 EXAFS parame	eters determined by	shell fitting of As K-ed	lge EXAFS spectra for	r As(V)	and Si adsorption on TiO2

样品	类型	CN/	R/nm	$\sigma^2/\mathrm{nm}$	$\Delta E/\mathrm{eV}$	R-factor
25.0	As—O	4 ± 0.6	16.8 ± 0.012	$0.021 \pm 0.017$	$3.0 \pm 2.0$	0.033
As(V)	As—0—0	12	$30.6 \pm 0.02$	AL.	$3.0 \pm 2.0$	0.033
19 1/2	As—Ti	$0.8 \pm 1.6$	$33.0 \pm 0.48$	$0.033 \pm 0.175$	$3.0 \pm 2.0$	0.033
(0)	As—O	$4 \pm 0.5$	$16.9 \pm 0.1$	$0.019 \pm 0.014$	$5.4 \pm 1.4$	0.025
Si/As(V) = 10	As-O-O	12	$30.8 \pm 0.2$	_	$5.4 \pm 1.4$	0.025
40	As—Ti	$0.4 \pm 0.9$	$33.2 \pm 0.3$	$0.001 \pm 0.145$	$5.4 \pm 1.4$	0.025

#### 2.2 NaF对Si的脱附动力学

3 次循环中不同 NaF 浓度下 Si 的脱附动力学曲线如图 2 所示. 利用动力学模型对 Si 的脱附动力学数据进行拟合,发现准二级动力学模型能较好地拟合对 Si 的脱附动力学过程( $R^2 > 0.96$ ). 准二级动力学模型表达式为:

$$\frac{t}{q_t} = \frac{1}{kq_e^2} + \frac{t}{q_e}$$

式中,  $q_e$  和  $q_t$  分别为平衡时刻和 t 时刻的脱附率, t 为脱附时间(min), k 为准二级动力学模型的脱附速率常数(min<sup>-1</sup>). 拟合结果见图 2, 动力学拟合参数见表 2.

表 2 第1~3次 NaF 脱附 Si 准二级动力学模型拟合参数

Table 2 Desorption kinetics parameters of Si by NaF for three cycles

第1次脱附		第2次反洗			第3次反洗			
NaF 浓度 /mg·L <sup>-1</sup>	k	$R^2$	NaF 浓度 /mg·L <sup>-1</sup>	k	$R^2$	NaF 浓度 /mg·L <sup>-1</sup>	k	$R^2$
10	0. 024 5	0. 992 7	10	0. 006 7	0. 965 7	10	0. 009 4	0. 990 4
50	0.0096	0. 985 2	50	0.0043	0. 974 0	50	0.0056	0. 985 8
100	0.0091	0. 985 5	100	0.0040	0. 974 5	100	0.0088	0. 985 8
200	0.0154	0.9970	200	0.0089	0. 989 2	200	0.0100	0. 996 4
500	0.0530	0. 999 1	500	0.0192	0. 990 3	500	0.0990	0. 996 7

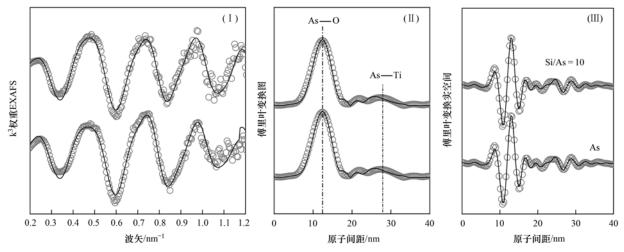


图 1 单砷和砷硅(摩尔比:Si/As = 10) 吸附在颗粒  $TiO_2$ 上的砷 K 边 EXAFS 谱图

Fig. 1 As K-edge EXAFS spectra of As(V) and As(V) in the presence of Si(OH)4 adsorption on TiO2 with the molar ratio of Si/As of 10

从图 2(a)~2(c)可知,3次反洗过程中,不同浓度 NaF 都能洗脱 TiO<sub>2</sub>表面吸附的 Si,说明 NaF 是一种有效的 Si 洗脱方法. TiO<sub>2</sub> 在反洗过程中比较稳定,洗脱液中并未检测到钛(Ti),说明洗脱过程中无 Ti 的溶出,NaF 反洗是一种安全的再生方法.比较 3 次循环中不同浓度 NaF 下脱附 Si 的动力学曲线,发现随 NaF 浓度增大,对应 Si 的脱附率逐渐

增高. NaF 浓度为 200 mg·L<sup>-1</sup>时, 3 次反洗中 Si 脱附率分别为 82.1% ± 1.47%、84.7% ± 2.14%、92.3% ± 2.47%,均在 80% 以上. 当 NaF 浓度为500 mg·L<sup>-1</sup>时, 3 次反洗中 Si 脱附率达到 95% 以上. 由图 2(d)可知, 3 次循环过程中,同一浓度的NaF 对 Si 的脱附率随反洗次数的增加略有增大,如500 mg·L<sup>-1</sup> NaF 在第 3 次反洗时对 Si 脱附率达到

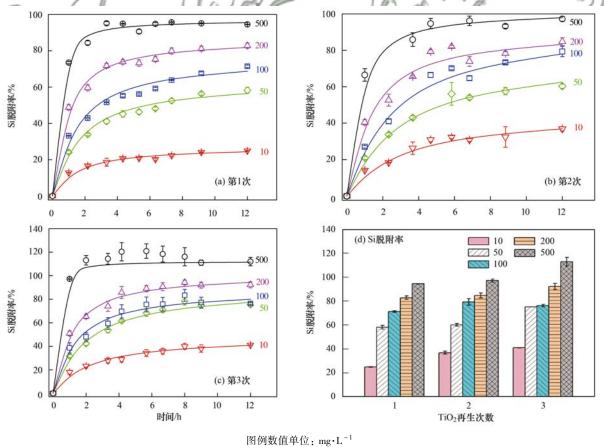


图 2 第 1~3 次 NaF 脱附 Si 的准二级动力学曲线模拟及总脱附率

Fig. 2 Desorption kinetic curves and final desorption rates of Si by NaF for three cycles

113% ±3.60%,明显高于第 1~2 次反洗时 Si 的脱附率(94.53% ±0.13%、97.24% ±1.32%). 推测原因可能是 NaF 第 1 次反洗 TiO<sub>2</sub> 时未能完全洗脱其表面的 Si,即 TiO<sub>2</sub> 表面仍残留有 Si 聚合体,当 NaF 再次反洗时,之前残留的 Si 聚合体可被进一步脱附,这就造成 Si 脱附率较前次反洗时增大. 在本实验体系中,认为 200 mg·L $^{-1}$  NaF 是最为经济且有效的 Si 洗脱剂浓度. 由图 2 可知,经 6 h 后脱附反应基本平衡,故脱附时间可控制在 6 h 内.

#### 2.3 Si 在 TiO<sub>2</sub> 上的微观吸附和脱附行为

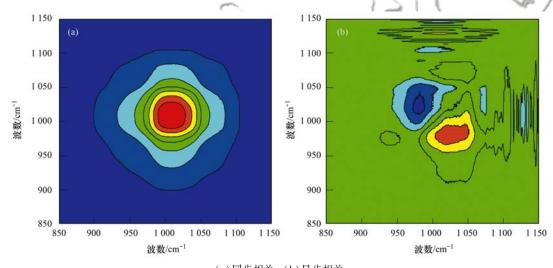
Si 溶液在 TiO<sub>2</sub> 薄膜上吸附 3.5 h, 对收集到的 谱图进行二维处理,可更进一步观察 Si 在 TiO<sub>2</sub> 上 的微观聚合行为<sup>[22,23]</sup>. 有关 Si 的特征峰描述见表 3, Si 单体是单体分子; Si 低聚体分为两种,一种为 双聚体 (Si<sub>2</sub>O<sub>7</sub><sup>6-</sup>), 另一种为环状聚合物,例如 (SiO<sub>3</sub><sup>2-</sup>)<sub>n</sub>, 其中 n 为 3、4 或 6; Si 多聚体是由多于 6 个的 Si 单体以不同结合方式构成的多样化分

子<sup>[20,21]</sup>. 对比同步[图 3(a)]、异步[图 3(b)]二维 红外相关光谱可知,同步和异步二维光谱图中 Si 特征峰均为正峰,说明位于 948 cm<sup>-1</sup>处 Si 单体的 出现要早于1 003 cm<sup>-1</sup>和1 110 cm<sup>-1</sup>处的 Si 低聚体和多聚体<sup>[24]</sup>. 吸附初始阶段,Si 主要以 Si 单体形式存在于 TiO<sub>2</sub>,随吸附时间的延长,Si 在 TiO<sub>2</sub> 表面主要以低聚体和多聚体形式稳定存在. 之前研究表明,Si 单体能够被As(V)解析,Si 的低聚体和多聚体因难以解析而一直稳定存在于 TiO<sub>2</sub> 表面<sup>[18]</sup>,所以寻找一种有效洗脱 Si 聚合体的方法成为必要.

#### 表 3 Si 在 $TiO_2$ 上吸附的 FTIR 特征峰位置 [24,25]

Table 3 FTIR peak positions and assignments

for adsorbed silicate on TiO2 波数/cm<sup>-1</sup> 波数/cm<sup>-1</sup> 特征峰描述 特征峰描述 Si 单体和低聚体 822 1 003 Si 低聚体 Si 单体和低聚体 1 010 851 Si 低聚体 948 Si 单体 1 110 Si 多聚体 Si 单体 Si 多聚体 955 1 118



(a) 同步相关; (b) 异步相关 图 3 Si 在  $TiO_2$  上吸附的同步和异步二维红外相关光谱

Fig. 3 Synchronous and asynchronous 2D IR spectra of Si adsorption on  ${\rm TiO_2}$ 

Si 溶液在 TiO<sub>2</sub> 薄膜上吸附 3.5 h 后, 脱附 0 h 和 3 h 的红外分峰结果谱图如图 4 所示. 从中可知, 当连续通入 50 mg·L<sup>-1</sup> NaF 溶液 3 h 后, 位于 822 cm<sup>-1</sup>的 Si 单体和低聚体振动峰向 851 cm<sup>-1</sup>处偏移, 位于 948 cm<sup>-1</sup>的 Si 单体振动峰向 955 cm<sup>-1</sup>处偏移, 这是由吸附过程中相邻基团之间的相互作用所导致的<sup>[24]</sup>. 将通入 NaF 溶液 0 h [图 4(a)]和 3 h [图 4(b)]的特征峰强对比, Si 单体位于 948 ~ 955 cm<sup>-1</sup>的 Si—O 和 Si 多聚体位于1111 ~ 1118 cm<sup>-1</sup>处的 Si—O—Si 特征峰明显减弱,说明 NaF 能够使吸附态 Si 单体和多聚体从 TiO<sub>2</sub> 上脱附,这就从微观界

面角度证明了 NaF 对 Si 聚合体的脱附效果.

#### 2.4 NaF与NaOH共同再生TiO,

在处理实际高砷地下水时,洗脱  $TiO_2$  表面吸附或聚合态的 As 和 Si 是吸附材料再生的关键. 之前研究表明, $80~g \cdot L^{-1}$  NaOH 可以有效脱附  $TiO_2$  表面吸附的 As,脱附率为  $98.7\% \sim 99.5\%$ ,但对 Si 的脱附率仅为  $45.9\% \sim 48.2\%^{[18]}$ . 本研究拟采用 NaOH 和 NaF 共同洗脱的方式再生  $TiO_2$  材料,即先 利用  $80~g \cdot L^{-1}$  NaOH 溶液反洗 4~h,然后利用  $200~mg \cdot L^{-1}$  NaF 反洗 6~h,对  $TiO_2$  进行 3~ 次再生以期探究其再生效果. 如图 5~ 所示,3~ 次循环中,As~ 的最

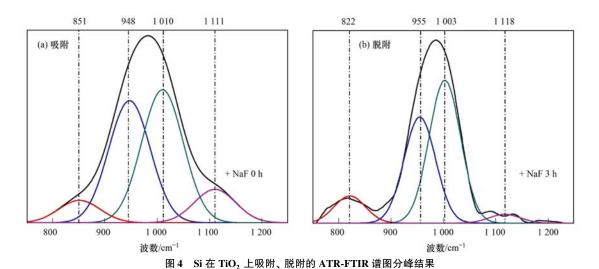


Fig. 4  $\,$  ATR-FTIR spectra and peak fitting results of Si adsorption and desorption on  ${\rm TiO_2}$ 

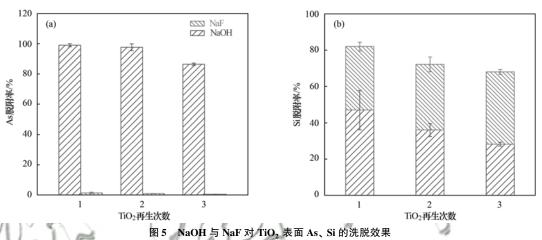


Fig. 5 Desorption rate of As and Si from  ${\rm TiO_2}$  by NaOH and NaF

终脱附率为 95. 2%  $\pm$  7. 4% , 均达到 85. 0% 以上. 分步反洗结果表明 NaOH 对 As 的脱附效果显著,而 NaF 对 As 几乎没有脱附效果. 3 次循环中 Si 最终脱附率为 74. 0%  $\pm$  7. 2% , NaOH 和 NaF 均对 Si 具有脱附效果,其中 NaOH 的脱附率分别为 46. 9%

 $\pm 10.7\%$ 、36.0%  $\pm 3.5\%$ 、28.2%  $\pm 1.0\%$ ,而后续 NaF 的加入使 Si 的脱附率提高了 34.9%  $\pm 2.4\%$ 、36.0%  $\pm 4.08\%$ 、39.7%  $\pm 1.3\%$ . 随着循环次数的增加, Si 的脱附率逐渐降低, 其原因可能是 NaOH 对 Si 脱附率逐渐降低, 因此在实际操作中

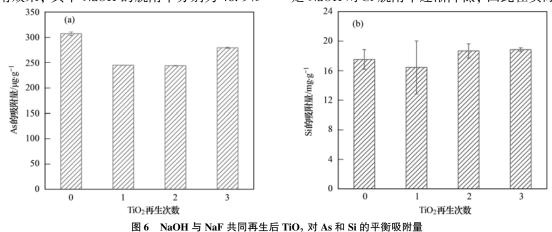


Fig. 6 Adsorption capacity of As and Si on TiO2 after the regeneration by NaOH and NaF

为达到更好的洗脱效果,可以考虑将 NaF 反洗液用量增大或延长 NaF 的反洗时间. 从图 6 可看出再生前后 TiO<sub>2</sub> 对 As 和 Si 的吸附量变化不大,表明再生后的 TiO<sub>2</sub> 吸附能力仍维持在一个较好的水平. 由此可见, NaOH 和 NaF 能够有效洗脱 TiO<sub>2</sub> 表面吸附或聚合态的 As 和 Si,释放由 As 和 Si 占据的吸附位点,达到 TiO<sub>2</sub>的再次回用.

#### 3 结论

- (1) Si 的存在不会影响 As( V) 在 TiO<sub>2</sub>上的微观吸附结构, Si 对As( V) 吸附的阻碍作用是由于竞争吸附位点引起的.
- (2) NaF 可稳定有效地洗脱 TiO<sub>2</sub> 表面吸附的 Si 聚合体, TiO<sub>3</sub> 在洗脱过程中性质稳定.
- (3) ATR-FTIR 结果显示 Si 在 TiO<sub>2</sub> 表面吸附时生成 Si 单体、Si 低聚体、Si 多聚体. 随着吸附时间的延长,Si 在 TiO<sub>2</sub> 表面主要以低聚体和多聚体形式存在. 通入 NaF 后,Si 单体和 Si 多聚体的特征峰降低,说明 NaF 能够使吸附态 Si 单体和多聚体从TiO<sub>2</sub> 上脱附下来.
- (4) NaOH 和 NaF 可有效洗脱 TiO<sub>2</sub> 表面吸附或聚合态的 As 和 Si, 3 次再生循环中 As 的脱附率为95.2%±7.4%, Si 脱附率为74.0%±7.2%, 再生后 TiO<sub>3</sub> 仍具有较强的吸附能力.

#### 参考文献:

- [1] Smith A. H., Lopipero P. A., Bates M. N., et al. Arsenic epidemiology and drinking water standards [J]. Science, 2002, 296 (5576): 2145-2146.
- [ 2 ] Rodríguez-Lado L, Sun G F, Berg M, et al. Groundwater arsenic contamination throughout China [ J ]. Science, 2013, 341 (6148): 866-868.
- [3] Nordstrom D K. Worldwide occurrences of arsenic in ground water [J]. Science, 2002, 296 (5576); 2143-2145.
- [4] Jain C K, Ali I. Arsenic: occurrence, toxicity and speciation techniques [J]. Water Research, 2000, 34 (17): 4304-4312
- [5] Sharma V K, Sohn M. Aquatic arsenic: toxicity, speciation, transformations, and remediation[J]. Environment International, 2009, 35(4): 743-759.
- [6] Mohan D, Pittman Jr C U. Arsenic removal from water/wastewater using adsorbents-a critical review [J]. Journal of Hazardous Materials, 2007, 142(1-2): 1-53.
- [7] Yan L, Hu S, Jing C Y. Recent progress of arsenic adsorption on TiO<sub>2</sub> in the presence of coexisting ions: a review[J]. Journal of Environmental Sciences, 2016, 49: 74-85.
- [8] Pena M, Meng X G, Korfiatis G P, et al. Adsorption mechanism of arsenic on nanocrystalline titanium dioxide[J]. Environmental Science & Technology, 2006, 40(4): 1257-1262.
- [ 9 ] Guan X H, Du J S, Meng X G, et al. Application of titanium dioxide in arsenic removal from water: a review[J]. Journal of Hazardous Materials, 2012, 215-216: 1-16.

- [10] Jing C Y, Meng X G, Calvache E, et al. Remediation of organic and inorganic arsenic contaminated groundwater using a nanocrystalline TiO<sub>2</sub>-based adsorbent [ J ]. Environmental Pollution, 2009, **157**(8-9): 2514-2519.
- [11] Cui J L, Du J J, Yu S W, et al. Groundwater arsenic removal using granular TiO<sub>2</sub>: integrated laboratory and field study [J]. Environmental Science and Pollution Research, 2015, 22(11): 8224-8234.
- [12] Laky D, Licskó I. Arsenic removal by ferric-chloride coagulation-effect of phosphate, bicarbonate and silicate [J]. Water Science & Technology, 2011, 64(5): 1046-1055.
- [13] Roberts L C, Hug S J, Ruettimann T, et al. Arsenic removal with iron( II ) and iron( III ) in waters with high silicate and phosphate concentrations [ J ]. Environmental Science & Technology, 2004, 38(1): 307-315.
- [14] Gao X D, Root R A, Farrell J, et al. Effect of silicic acid on arsenate and arsenite retention mechanisms on 6-L ferrihydrite; a spectroscopic and batch adsorption approach [J]. Applied Geochemistry, 2013, 38: 110-120.
- [15] Hu S, Yan W, Duan Y M. Polymerization of silicate on TiO<sub>2</sub> and its influence on arsenate adsorption: an ATR-FTIR study [J]. Colloids and Surfaces A: Physicochemical and Engineering Aspects, 2015, 469: 180-186.
- [16] Hiemstra T, Barnett M O, Van Riemsdijk W H. Interaction of silicic acid with goethite [J]. Journal of Colloid and Interface Science, 2007, 310(1): 8-17.
- [17] Yang X F, Roonasi P, Jolster? R, et al. Kinetics of silicate sorption on magnetite and magnemite; an in situ ATR-FTIR study [J]. Colloids and Surfaces A; Physicochemical and Engineering Aspects, 2009, 343(1-3): 24-29.
- Aspects, 2009, 343(1-3); 24-29.

  [18] Hu S, Shi Q T, Jing C Y. Groundwater arsenic adsorption on granular TiO<sub>2</sub>: integrating atomic structure, filtration, and health impact [J]. Environmental Science & Technology, 2015, 49 (16): 9707-9713.
- [19] 谢冬梅,曹林洪,崔金立. 二氧化钛颗粒制备及其对水中三价砷的去除[J]. 环境工程学报, 2013, 7(4): 1279-1284. Xie D M, Cao L H, Cui J L. Preparation and evaluation of TiO<sub>2</sub> granule for As(Ⅲ) removal from water[J]. Chinese Journal of Environmental Engineering, 2013, 7(4): 1279-1284.
- [20] Luxton T P, Eick M J, Rimstidt D J. The role of silicate in the adsorption/desorption of arsenite on goethite [J]. Chemical Geology, 2008, 252(3-4): 125-135.
- [21] Christl I, Brechbühl Y, Graf M, et al. Polymerization of silicate on hematite surfaces and its influence on arsenic sorption [J]. Environmental Science & Technology, 2012, 46 (24): 13235-13243.
- [22] Noda I. Close-up view on the inner workings of two-dimensional correlation spectroscopy [J]. Vibrational Spectroscopy, 2012, 60: 146-153.
- [23] Ernst R R, Bodenhausen G, Wokaun A. Principles of nuclear magnetic resonance in one and two dimensions [M]. Oxford: Oxford University Press, 1987. 253-253.
- [24] Swedlund P J, Miskelly G M, McQuillan A J. An attenuated total reflectance IR study of silicic acid adsorbed onto a ferric oxyhydroxide surface [J]. Geochimica et Cosmochimica Acta, 2009, 73(14): 4199-4214.
- [25] Swedlund P J, Song Y T, Zujovic Z D, et al. Short range order at the amorphous TiO<sub>2</sub>-water interface probed by silicic acid adsorption and interfacial oligomerization; an ATR-IR and <sup>29</sup>Si MAS-NMR study[J]. Journal of Colloid and Interface Science, 2012, 368(1); 447-455.

## **HUANJING KEXUE**

Environmental Science (monthly)

Vol. 39 No. 3 Mar. 15, 2018

### **CONTENTS**

Characterization and Variation of Organic Carbon (OC) and Elemental Carbon (EC) in PM <sub>2.5</sub> During the Winter in the Yangtze Fi	tiver Delta Region, China ·····
Characterization and Variation of Organic Galloon (OC) and Electrical California (ED) in Fig. 5 During the Winter in the Fangue Fig.	
Important Effect of Secondary Inorganic Salt Extinction on Visibility Impairment in the Northern Suburb of Nanjing	
Day-Night Differences and Source Apportionment of Inorganic Components of PM <sub>2.5</sub> During Summer-Winter in Changzhou City ·····	······ LIU Jia-shu, GU Yuan, MA Shuai-shuai, et al. (980)
Characteristics of Elements in PM <sub>2.5</sub> and PM <sub>10</sub> in Road Dust Fall During Spring in Tianjin	······ WANG Shi-bao, JI Ya-qin, LI Shu-li, et al. (990)
Particle Size Distribution and Human Health Risk Assessment of Heavy Metals in Atmospheric Particles from Beijing and Xinxiang	During Summer
	····· ZHANG Xin, ZHAO Xiao-man, MENG Xue-jie, et al. (997)
$ Ecological \ and \ Health \ Risks \ of \ Trace \ Heavy \ Metals \ in \ Atmospheric \ PM_{25} \ Collected \ in \ Wuxiang \ Town, \ Shanxi \ Province $	····· GUO Zhao-xia, GENG Hong, ZHANG Jin-hong, et al. (1004)
Characteristics of Particulate and Inorganic Elements of Motor Vehicles Based on a Tunnel Environment	
A 2013-based Atmospheric Ammonia Emission Inventory and Its Characteristic of Spatial Distribution in Henan Province	
Emission Characteristics of Wind Erosion Dust from Topsoil of Urban Roadside-Tree Pool	····· LI Bei-bei, QIN Jian-ping, QI Li-rong, et al. (1031)
Particulate Component Emission Characteristic from a Diesel Bus with DOC and CDPF	······ LOU Di-ming, GENG Xiao-yu, SONG Bo, et al. (1040)
Water Quality in the Henan Intake Area of the South-to-North Water Diversion Project	
Spatio-Temporal Patterns and Environmental Risk of Endocrine Disrupting Chemicals in the Liuxi River	······ FAN Jing-jing, WANG Sai, TANG Jin-peng, et al. (1053)
Fate and Origin of Major Ions in River Water in the Lhasa River Basin, Tibet	······ ZHANG Qing-hua, SUN Ping-an, HE Shi-yi, et al. (1065)
Identification of Nitrate Sources and the Fate of Nitrate in Downstream Areas: A Case Study in the Taizi River Basin	
Sources, Distribution of Main Controlling Factors, and Potential Ecological Risk Assessment for Heavy Metals in the Surface Sedim	ent of Hainan Island North Bay, South China
ZE	
Characteristics of Heavy Metals Pollution of Farmland and the Leaching Effect of Rainfall in Tianjin	
Seasonal Difference in Water Quality Between Lake and Inflow/Outflow Rivers of Lake Taihu, China	ZHA Hui-ming, ZHU Meng-yuan, ZHU Guang-wei, et al. (1102)
Characteristics of Nitrogen Release at the Sediment-Water Interface in the Typical Tributaries of the Three Gorges Reservoir During	the Sensitive Period in Spring
Spatial Distributions of Transferable Nitrogen Forms and Influencing Factors in Sediments from Inflow Rivers in Different Lake Basin	
Effects of Hydrological and Meteorological Conditions on Diatom Proliferation in Reservoirs	
Vertical Distribution of Fungal Community Composition and Water Quality During the Deep Reservoir Thermal Stratification S	
Community Structure and Influencing Factors of Bacterioplankton in Spring in Zhushan Bay, Lake Taihu	XUE Yin-gang, LIU Fei, SUN Meng, et al. (1151)
Characteristics of Sediment Oxygen Demand in a Drinking Water Reservoir	SU Lu, HUANG Ting-lin, LI Nan, et al. (1159)
Effects of Wastewater Nitrogen Concentrations and NH <sub>4</sub> <sup>+</sup> /NO <sub>3</sub> <sup>-</sup> on Nitrogen Removal Ability and the Nitrogen Component of Myriop	hyllum aquaticum (Vell.) Verde ·····
4 3 0 7 0 1 7 1	··· MA Yong-fei, YANG Xiao-zhen, ZHAO Xiao-hu, et al. (1167)
Effect of Nutrient Loadings on the Regulation of Water Nitrogen and Phosphorus by Vallisneria natans and Its Photosynthetic Fluores	scence Characteristics ·····
Enter of Francisco and To Topical of Water Francisco and Transporter by Francisco and To Topical of Transporter by Francisco and To Topical of Topical of Transporter by Francisco and Topical of Topi	···· ZHOU Yi-wen, XU Xiao-guang, HAN Rui-ming, et al. (1180)
Removal of Organic Matter from Water by Chemical Preoxidation Coupled with Biogenic Manganese Oxidation	··· JIAN Zhi-yu, CHANG Yang-yang, WANG Li-xin, et al. (1188)
Treating Simulated Dye Wastewater by an In Situ Copper Ferrite Process	······· HAN Zhi-yong, HAN Kun, HAO Hao-tian, et al. (1195)
Experiment to Enhance Catalytic Activity of α-FeOOH in Heterogeneous UV-Fenton System by Addition of Oxalate	·· MIAO Xiao-zeng, DAI Hui-wang, CHEN Jian-xin, et al. (1202)
Fabrication of a Biomass-Based Hydrous Zirconium Oxide Nanocomposite for Advanced Phosphate Removal	QIU Hui, QIN Zhi-feng, LIU Feng-ling, et al. (1212)
Characteristic of Nitrate Adsorption in Aqueous Solution by Iron and Manganese Oxide/Biochar Composites	· ZHENG Xiao-qing, WEI An-lei, ZHANG Yi-xuan, et al. (1220)
Preparation of PAAm/HACC Semi-Interpenetrate Network Hydrogel and Its Adsorption Properties for Humic Acid from Aqueous Sol	
Groundwater Arsenic and Silicate Adsorption on TiO <sub>2</sub> and the Regeneration of TiO <sub>2</sub>	MA Wen-jing, YAN Li, ZHANG Jian-feng ( 1241 )
Removal Efficiency and Mechanism of Removal by Humic Acid of the Integrated Floc-ultrafiltration Process	
Emission Inventory of Greenhouse Gas from Urban Wastewater Treatment Plants and Its Temporal and Spatial Distribution in China	··········· YAN Xu, QIU De-zhi, GUO Dong-li, et al. (1256)
Start-up and Operation of Biofilter Coupled Nitrification and CANON for the Removal of Iron, Manganese and Ammonia Nitrogen ·	LI Dong, CAO Rui-hua, YANG Hang, et al. (1264)
Analysis of CANON Process Start-up with Fiber Carrier	GU Cheng-wei, CHEN Fang-min, LI Xiang, et al. (1272)
Characteristics of Biofilm During the Transition Process of Complete Nitrification and Partial Nitrification	
Effect of Intermediate-Setting Aeration on the CANON Granular Sludge Process in the AUSB Reactor	CHENG Shuo, LI Dong, ZHANG Jie, et al. (1286)
Effect of Organic Carbon Source on Start-up and Operation of the CANON Granular Sludge Process	LI Dong, WANG Yan-ju, LÜ Yu-feng, et al. (1294)
Start-Up and Regional Characteristics of a Pilot-scale Integrated PN-ANAMMOX Reactor	
Effect of NO, -N Recycling Ratio on Denitrifying Phosphorus Removal Efficiency in the ABR-MBR Combined Process	
Effects of Magnetic Fe <sub>3</sub> O <sub>4</sub> Nanoparticles on the Characteristics of Anaerobic Granular Sludge and Its Interior Microbial Community	
Characterization Composition of Soluble Microbial Products in an Aerobic Granular Sludge System	
Influence of Ciprofloxacin on the Microbial Community and Antibiotics Resistance Genes in a Membrane Bioreactor	
Analysis of Low C/N Wastewater Treatment and Structure by the CEM-UF Combined Membrane-Nitrification/Denitrification System	
	· XING lin-liang, ZHANG Yan, CHEN Chang-ming, et al. (1342)
Effects of Phosphorus on the Activity and Bacterial Community in Mixotrophic Denitrification Sludge	
Acclimatization and Community Structure Analysis of the Microbial Consortium in Nitrate-Dependent Anaerobic Methane Oxidation	1, , , , ,
Diffusion of Microorganism and Main Pathogenic Bacteria During Municipal Treated Wastewater Discharged into Sea	
Oxytetracycline Wastewater Treatment in Microbial Fuel Cells and the Analysis of Microbial Communities	
Spatial and Temporal Variability of Soil C-to-N Ratio of Yugan County and Its Influencing Factors in the Past 30 Years	
Spatial Heterogeneity of Soil Carbon and its Fractions in the Wolfberry Field of Zhongning County	
Response of Soil Enzyme Activities and Their Relationships with Physicochemical Properties to Different Aged Coastal Reclamation	
recoponed or con analytic recurred and then rectanonemps with rhysicoenical rioperies to different riger Coastal rectalliation	VIE Vuo fong DILLi iio WANC Oi gi et al. (1404)
Distribution, Sources, and Ecological Risk Assessment of Polycyclic Aromatic Hydrocarbons (PAHs) in Soils of the Central and E	astern Areas of the Oinghai-Tibetan Plateau ·····
Distribution, Sources, and Ecological Risk Assessment of Polycyclic Aromatic Hydrocarbons (PAHs) in Soils of the Central and E	astern Areas of the Qinghai-Tibetan Plateau
Distribution, Sources, and Ecological Risk Assessment of Polycyclic Aromatic Hydrocarbons (PAHs) in Soils of the Central and E  Source Apportionment of Heavy Metals in Farmland Soils Around Mining Area Based on UNMIX Model	astern Areas of the Qinghai-Tibetan Plateau
Distribution, Sources, and Ecological Risk Assessment of Polycyclic Aromatic Hydrocarbons (PAHs) in Soils of the Central and E	astern Areas of the Qinghai-Tibetan Plateau